JOURNAL OF COMPUTATIONAL PHYSICS 6, 168–182 (1970)

Transonic Flows Past a Circular Cylinder

CZESLAW P. KENTZER[1]

Purdue University, West Lafayette, Indiana 47907

Received November 11, 1969; revised January 30, 1970

Impulsively started, time-dependent inviscid transonic flows past a circular cylinder are considered for the case of a symmetric flow of an ideal compressible gas. A finite-difference method is applied to an annular region between the cylinder and the gasdynamic discontinuity created by a sudden immersion of the cylinder into the uniform stream. Numerical solutions are presented for the transonic free stream. A discussion of factors affecting the accuracy is given. It is concluded that imbedded shocks, if present, must be treated as discontinuities in order to maintain a reasonable accuracy.

INTRODUCTION

Recent years witnessed a rebirth of interest in transonic aerodynamics. Mathematical difficulties connected with an analytical treatment of the problem continue to hinder the progress in computation of transonic flows. As a natural consequence, many researchers turned to numerical methods. The experience, gained in the numerical solution of the supersonic blunt body problem during the last decade, proved valuable in attacking the related problem of the transonic flow, both problems being governed by mixed-type equations in the steady case. It is, therefore, not surprising that a method originally developed for the supersonic blunt body flows, e.g., the method of integral relations [1], was used with success by Chushkin in solving the problem of a sonic flow past cylinders [2]. The difficulty of obtaining numerical solutions for Mach numbers less than unity, but higher than the critical value, was overcome recently with finite-difference time-dependent methods by Singleton [3], and by Magnus, Gallaher and Yoshihara [4]. The common feature of the finite-difference solutions is that they could be applied to a well-posed initial-value problem for the time-dependent case. However, the central difficulty arising in calculations of unconfined flows is the proper imposition of the boundary conditions at infinity. Artificial conditions, corresponding to fixed, permeable, subsonic boundaries at a finite distance from the body, render the problem ill-posed.

[1] Associate Professor, School of Aeronautics, Astronautics and Engineering Sciences.

Recently the author has formulated a general problem of computing impulsively started, external flows on an infinite domain [5]. Starting with the premise that the natural external boundary of a flow disturbed by a body suddenly immersed in it is a gasdynamic discontinuity propagating outwards from the body, it is sufficient to calculate the time-dependent solution only on the inside of the annular region between the body and the outward-moving disturbance. The motion of the latter is governed by the exact Rankine–Hugoniot jump conditions. The annular domain of integration remains finite in extent for all times less than infinity.

Numerical Method

The details of the method will be published separately [5]. For completeness, the main features of the method are discussed briefly here. The task is to integrate numerically the partial differential equations of gasdynamics with respect to time over the annular region between the cylinder of radius R and the moving gasdynamic discontinuity, subject to initial and boundary conditions. The system of equations considered is

$$\frac{\partial \rho}{\partial t} = -\left[u\frac{\partial \rho}{\partial x'} + v\frac{\partial \rho}{\partial y'} + \rho\left(\frac{\partial u}{\partial x'} + \frac{\partial v}{\partial y'}\right)\right], \tag{1a}$$

$$\frac{\partial u}{\partial t} = -\left[u\frac{\partial u}{\partial x'} + v\frac{\partial u}{\partial y'} + \frac{1}{\rho}\frac{\partial p}{\partial x'}\right], \tag{1b}$$

$$\frac{\partial v}{\partial t} = -\left[u\frac{\partial v}{\partial x'} + v\frac{\partial v}{\partial y'} + \frac{1}{\rho}\frac{\partial p}{\partial y'}\right], \tag{1c}$$

$$\frac{\partial p}{\partial t} = -\left[u\frac{\partial p}{\partial x'} + v\frac{\partial p}{\partial y'} + \gamma p\left(\frac{\partial u}{\partial x'} + \frac{\partial v}{\partial y'}\right)\right], \tag{1d}$$

where the dependent variables are ρ = density, u, v = Cartesian components of velocity, p = pressure. Here γ = constant ratio of specific heats. Note that no assumption is made as to the constancy of entropy. Further, the temperature, energy, entropy, and other functions of interest are expressible in terms of the dependent variables through appropriate defining relations and need not be considered here.

Since the domain of integration is time-dependent, it is convenient to employ a curvilinear, nonorthogonal floating mesh spanning the annular region, Fig. 1a. A computer generated sequence of coordinate transformations maps the floating mesh on a rectangular domain, Fig. 1b, divided into a fixed, evenly spaced, rectangular mesh of $I \times J$ mesh points with coordinates x_i, y_j, $i = 1, 2,..., I$, $j = 1, 2,..., J$. The sequence of transformations employed mapped the Cartesian

coordinates, (x', y'), first into polar coordinates, (r, θ). The polar radius r was then replaced by $Q = 1 - R/r$, and the modified coordinates (Q, θ) were then normalized by referring them to their ranges: $x = \theta/\pi$, $y = Q/Q_s(\theta, t)$, where $Q_s = 1 - R/r_s(\theta, t)$ and $r = r_s$ is the equation of the shock wave. The interior boundary (the surface of the cylinder) is given by $y = 0$, and the exterior boundary (the discontinuity) by $y = 1$, while $x = 1$ and $x = 0$ correspond to the axis of symmetry upstream and downstream of the cylinder, respectively.

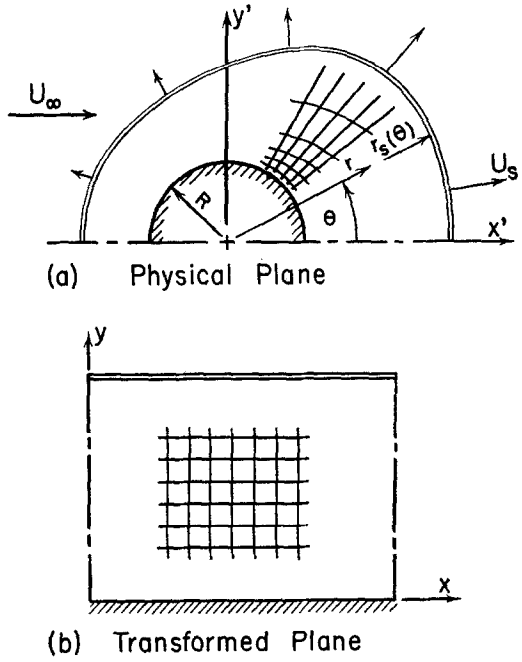

FIG. 1. Notation.

The Cartesian velocity components, u and v, are not subjected to the coordinate transformations. As a consequence, the spatial derivatives appearing in Eqs. (1) may be calculated conveniently by the Chain Rule of differentiation coded as a subroutine. The sequence of transformations of coordinates may be generated numerically by, first, storing proper numerical values of the elements of the transformation tensor, then calling the subroutine, and repeating the process a desired number of times. All the finite-difference approximations of spatial derivatives are applied in the transformed plane on the rectangular, equally divided mesh. The temporal derivatives are then available by a numerical evaluation of the right sides of Eqs. (1).

The choice of a particular finite-difference approximation is of no great consequence in a preliminary numerical study such as the present one provided that the chosen finite-difference scheme is consistent and stable. Because of the interest of the author in the role of truncation errors and in the fluid-mechanical interpretation of their influence on the numerical solution, it was decided to employ the following set of finite-difference expressions:

$$\frac{\partial f}{\partial t} = [f_{i,j}^{n+1} - f_{i,j}^{n-1}]/2\Delta t + g_{i,j}^{n},$$

$$\frac{\partial f}{\partial x} = [f_{i+1,j}^{n} - f_{i-1,j}^{n}]/2\Delta x,$$

$$\frac{\partial f}{\partial y} = [f_{i,j+1}^{n} - f_{i,j-1}^{n}]/2\Delta y,$$

where f is any one of the dependent variables: $u, v,$ = velocity components, p = pressure, ρ = density, and where the notation:

$$f_{i,j}^{n} = f(x_i, y_j, t_n) = f(i\Delta x, j\Delta y, n\Delta t)$$

is used. For the purpose of controlling the amount of numerical dissipation, the following expression was used for $g_{i,j}^{n}$:

$$g_{i,j}^{n} = \Big[\frac{\sigma}{2}(f_{i,j}^{n+1} - 2f_{i,j}^{n} + f_{i,j}^{n-1}) - \frac{\sigma}{4}(f_{i+1,j}^{n} + f_{i-1,j}^{n} - 4f_{i,j}^{n} + f_{i,j+1}^{n} + f_{i,j-1}^{n})\Big]\Big/\Delta t,$$

where σ is a weight factor treated as an arbitrary function of position or time. The above finite-difference scheme results from taking a weighted average of stable dissipative and nondissipative schemes. Linear stability analysis leads to the well-known Courant–Friedrichs–Lewy stability criterion provided that $0 \leqslant \sigma \leqslant 1$. Maximum numerical dissipation, as measured by truncation errors of second order, is present when $\sigma = 1$ and the dissipation is zero when $\sigma = 0$. In the latter case, only a marginal (neutral) stability is realized. In practice, one is limited to the range $0.01 \leqslant \sigma \leqslant 1$.

The following boundary conditions must be imposed on the solution:

1. tangency of the flow at the cylinder surface,
2. symmetry conditions on the axis of symmetry,
3. the Rankine–Hugoniot jump conditions on the moving discontinuity.

Special care was exercised in treating the boundary conditions on the body

and on the shock wave. The original ideas of Moretti [6], who first suggested treating finite-difference approximations of boundary conditions "in the spirit of the theory of characteristics," were used also in the present case.

Initial conditions were chosen so as to satisfy the boundary conditions and to represent a physically realistic yet simple impulsive starting of the flow. Taking the initial position of the discontinuity (the outer boundary) to be a circle concentric with the cylinder and of only slightly larger radius, it was assumed that fluid particles in front of the cylinder could move only in a direction tangential to the surface of the cylinder. Requiring that the discontinuity be a shock wave which leaves behind a velocity with zero component normal to the cylinder surface and using the Rankine–Hugoniot jump conditions, pressure, density and tangential component of velocity at the shock as well as the speed of the discontinuity were determined uniquely. Assuming that the density and velocity remain constant across the annulus between the body and the shock wave, integration of the conservation equation for the normal component of momentum gave a pressure distribution between the shock and the body. As a consequence, realistic conditions, corresponding in concept to the hypersonic Newtonian shock layer, were arrived at in front of the body. Further, assuming that fluid particles behind the cylinder continue to move with free stream velocity in the downstream direction until overtaken by an expansion wave, it was found sufficient to initiate the expansion by modifying only the velocity distribution at the cylinder surface where the velocity component normal to the surface was set equal to zero and the tangential component was set equal to the projection of the free stream velocity onto the surface. Since the discontinuity downstream of the body produced no change in flow conditions, its speed was set equal to the speed of an acoustic wave. The above procedures for the determination of convenient initial conditions in front and behind the cylinder are compatible with each other at the top of the cylinder and yield free stream conditions at the body and along the radial line up to and including the discontinuity which propagates upwards with the speed of sound.

The weighted sum (a linear combination) of dissipative and nondissipative schemes used allowed for local control of the numerical accuracy. As it may be shown easily, the leading term in the expression for the truncation error is introduced by the finite-difference expressions for the temporal derivatives. This term is in each of the Eqs. (1):

$$\frac{\sigma \Delta t}{2}\left\{\frac{\partial^2 f}{\partial t^2} - \frac{1}{2}\left[(\Delta x/\Delta t)^2 \frac{\partial^2 f}{\partial x^2} + (\Delta y/\Delta t)^2 \frac{\partial^2 f}{\partial y^2}\right]\right\},$$

where $f = \rho$, u, v, or p. It was found in practice that the weight factor σ could be kept as low as $\sigma = 0.01$ reducing the truncation error of the first order accuracy scheme by a factor of 100. However, the appearance of imbedded recompression

shocks in the transonic case caused rather severe oscillations of the solution. This was partially remedied by increasing the weight factor σ locally. Since schemes of higher (e.g., second) order accuracy also have a tendency to produce oscillations in presence of shock waves, the attempts at improving numerical accuracy were postponed until techniques are developed for handling imbedded shocks as surfaces of discontinuity.

The stability of numerical solutions, safe for occasional rapid growth of errors accumulated at the outer boundary, was maintained by observing the Courant–Friedrichs–Lewy linear stability criterion. For the present scheme on a floating mesh the following was used in arriving at a safe time step

$$\Delta t = 1/\{v_{\max}[(1/\Delta x')^2 + (1/\Delta y')^2]^{1/2}\}, \qquad 0.01 \leqslant \sigma \leqslant 1.00,$$

where $v_{\max} = [(u - u_m)^2 + (v - v_m)^2]^{1/2} + a$ = maximum speed of propagation of acoustic disturbances relative to the floating mesh, and where u_m, v_m are the Cartesian components of velocity of the floating mesh at the point in question, and a is the adiabatic speed of sound.

Numerical Examples

To aid in interpreting enclosed figures, we first note some common features of all late-time flows (excluding initial transients). Independently of the free-stream Mach number, the Mach number contour maps covering the annular region between the outward-moving discontinuity and the body may be divided into three zones by passing $M = M_\infty$ = constant lines between the body and the shock. On the body, there are two points where the local Mach number is equal to the free-stream Mach number, M_∞. The Mach number at the shock wave must be less than M_∞ in front of the body, larger than M_∞ above and downstream from the body, and equal to M_∞ on the axis in the wake region (unless numerical

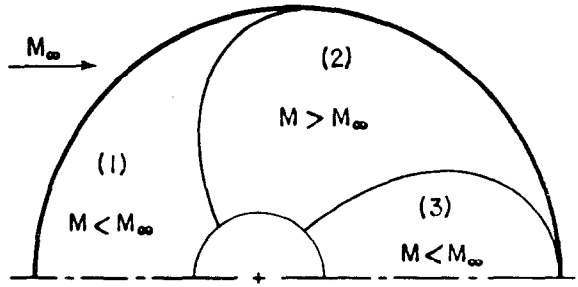

Fig. 2. Common features of constant Mach number contour maps (schematic).

dissipation and/or the presence of secondary shocks produce substantial entropy wake behind the cylinder). Thus, in front of the body we have a zone with $M < M_\infty$, denoted by (1), Fig. (2), above and downstream of the body we have a zone with $M > M_\infty$, denoted by (2), and in the wake region a zone with $M < M_\infty$ occurs again and is denoted by (3).

Conventional definitions of a transonic free stream lose their meaning when blunt bodies and time-dependent flows are considered. Unlike pointed bodies, blunt bodies will generate flows containing zones in which local velocities, relative to the body, will remain always smaller in magnitude than the local speed of sound. This must certainly be true near the front and rear stagnation points. The presence, or absence, and the spatial extent of a zone of supersonic flow may be used to distinguish between subsonic, transonic and supersonic flow. Consequently, we shall adopt in the sequel the following definition of transonic

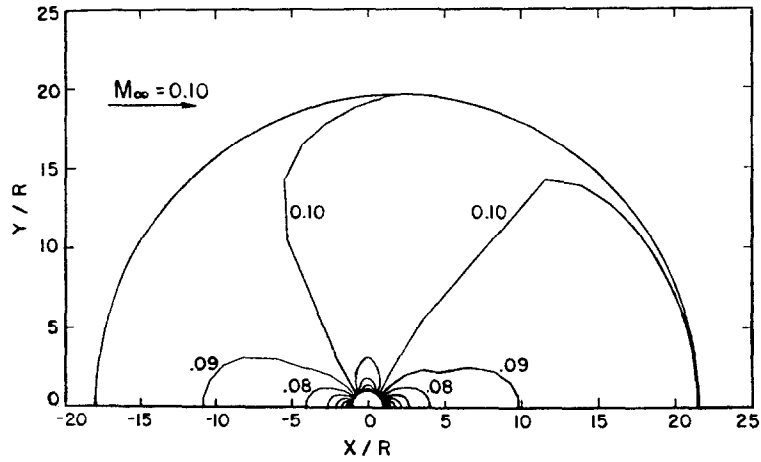

FIG. 3. Mach number contours, $M = 0.10$, $tU/R = 1.8$.

flows. By a transonic flow we shall mean a flow with the free-stream Mach number, relative to the body, such that in the limit of a steady flow there exist supersonic velocities confined to a local zone (or zones) of finite extent. Subsonic flows will be defined as flows with free-stream Mach number such that no imbedded supersonic zones exist in the limit of infinite time. By supersonic flow we shall mean a flow with a free-stream Mach number sufficiently high so that zones of supersonic flow extend between the body and the exterior boundary completely separating the front and rear subsonic zones in the limit as the exterior boundary is removed to infinity. The above definitions adopted here limit transonic flows proper to the range between the critical Mach number and $M_\infty = 1$. Supersonic

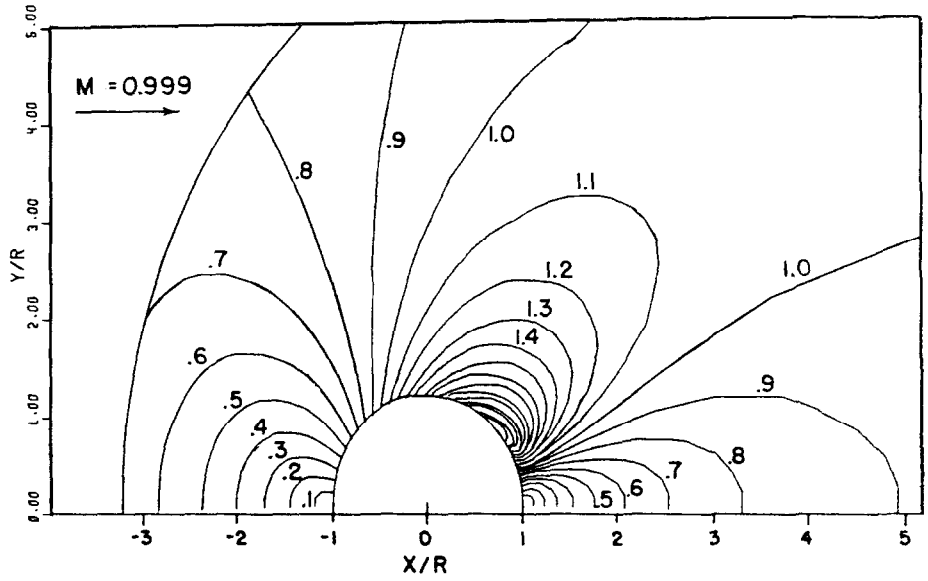

FIG. 4. Mach number contours, $M = 0.999$, $tU/R = 5.5$.

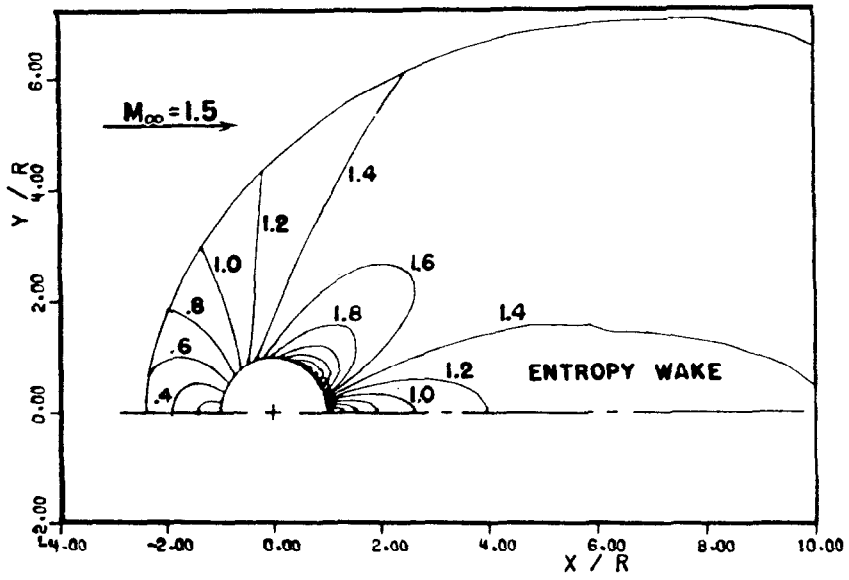

FIG. 5. Mach number contours, $M = 1.50$, $tU/R = 8.9$.

flows, as defined above, are characterized by the inability of acoustic signals, emanating from the neighborhood of the rear stagnation point, to travel upstream and influence the flow near the front stagnation point.

In subsonic flows an almost symmetric Mach number contour map results, Fig. (3), indicating small drag. The flow is almost steady and isentropic in the neighborhood of the body so that constant Mach number lines are also, approximately, the lines of constant pressure and density. When the local Mach number exceeds unity on the body, the symmetry is destroyed due to the overexpansion of the flow, Fig. (4). In transonic flow, $M_\infty < 1$, the sonic line is located in Zone 2. An almost sonic flow, $M_\infty = 0.999$, is shown in Fig. (4). At $M_\infty = 1$ the sonic

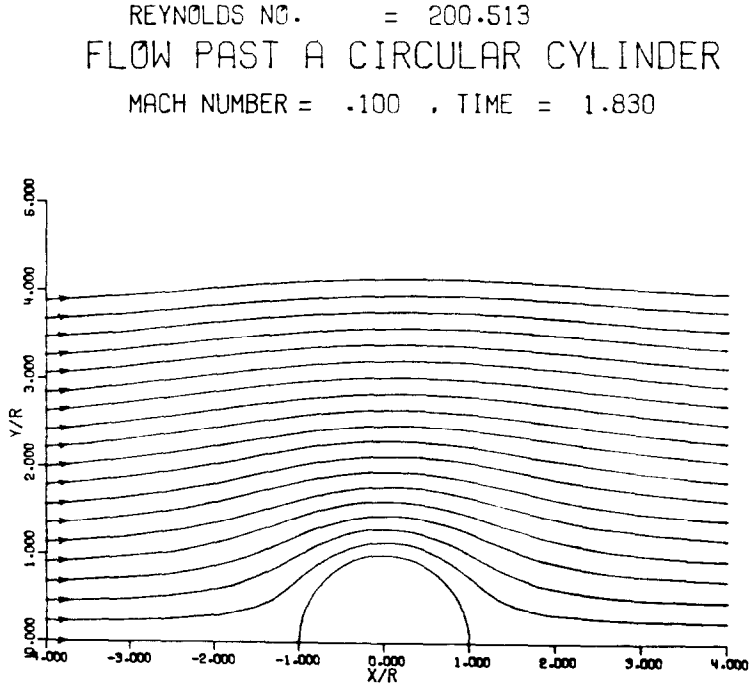

FIG. 6. Instantaneous streamlines, $M = 0.10$, $tU/R = 1.8$.

line is the dividing line between Zone 1 and 2. When supersonic flow is reached, the sonic line moves to Zone 1, Fig. (5).

The appearance of imbedded recompression shocks in the transonic and supersonic cases is not too obvious due to strong "smoothing" effects of the numerical dissipation. A better indication of the presence of shock waves is provided by constant stream function lines in Figs. (6)–(9). The stream function

does not satisfy the mass continuity equation due to a nonstationary character of the flow. However, the instantaneous streamlines (lines of constant mass flow) are tangent to the instantaneous velocity field. Consequently, sudden changes in the direction of the "streamlines" signal the presence of the recompression shock. No attempt was made to improve the numerical resolution of the imbedded shock waves.

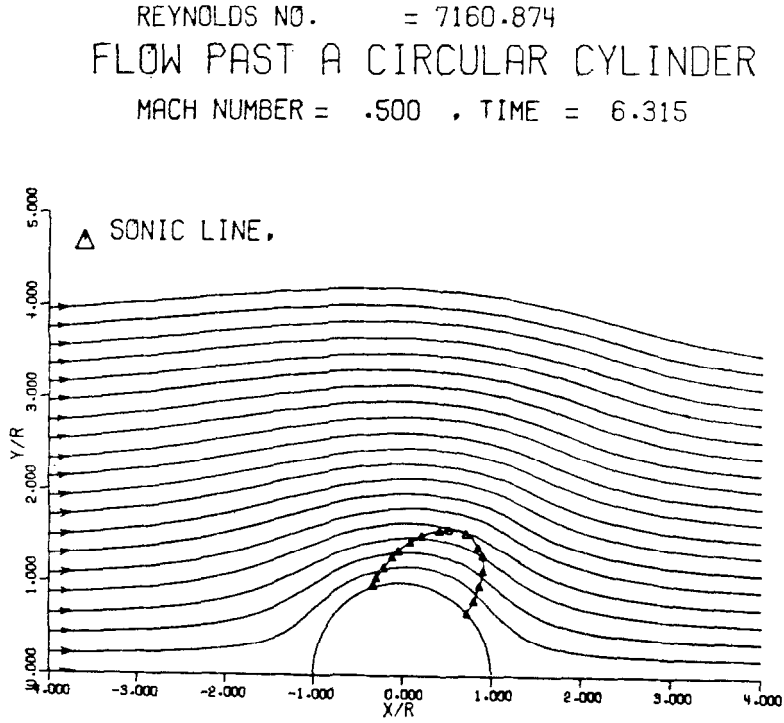

FIG. 7. Instantaneous streamlines, $M = 0.50$, $tU/R = 6.3$.

The case $M = 0.999$ illustrates both the generality and the limitations of the present formulation. Due to the fact that the solution must depend continuously on the boundary conditions, in particular on the Mach number, the solution for $M = 0.999$ has the same general features as supersonic and lower subsonic solutions. The primary limitation of the present solutions is their admittedly poor accuracy. The preliminary results reported here will serve, it is hoped, to point out where improvements in the method could be made in order to achieve satisfactory accuracy.

Figures 10 and 11 illustrate the convergence of numerical results with respect

to the mesh size and with respect to time (or number of integration steps). For the first 500 integration steps, 18 equal subdivisions were used along the upper surface of the cylinder; and only five unequal subdivisions were employed between the cylinder and the moving discontinuity. When the number of integration steps, N, exceeded 500, a finer mesh of 10 radial and 54 angular subdivisions was used. The sudden reduction of the mesh size lowered the numerical dissipation

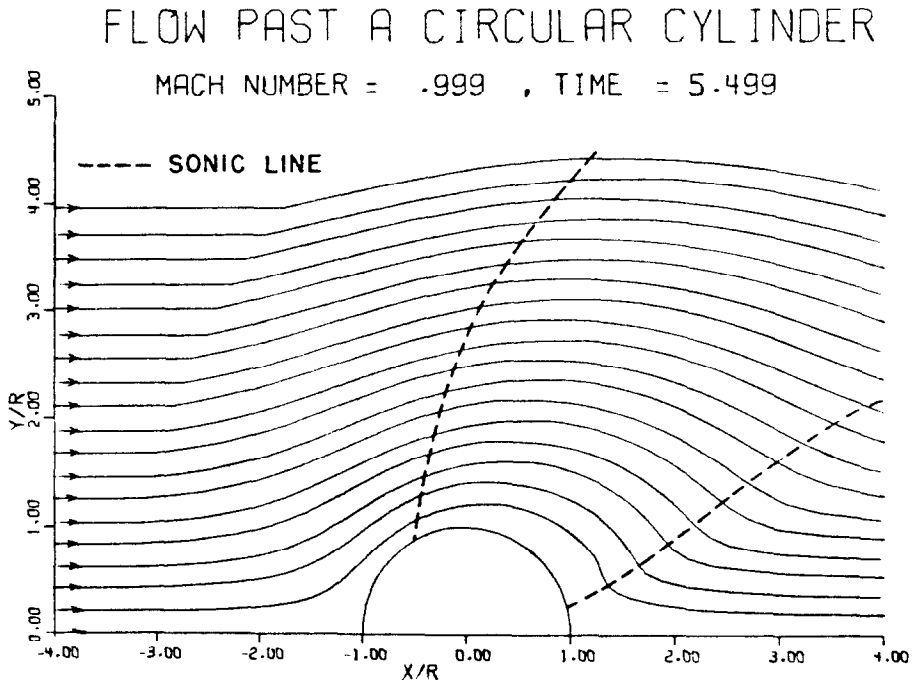

FIG. 8. Instantaneous streamlines, $M = 0.999$, $tU/R = 5.5$.

by a factor of 3.16. The velocity distribution, Fig. 10, responded to this change by quickly approaching a new asymptote. The difference between velocity distribution at $N = 600$ and $N = 700$ is small. Further improvement in accuracy could be attained not so much by integrating for many more hundreds of cycles as by increasing the number of subdivisions or by allowing for a discontinuous jump in the velocity at the downstream boundary of the supersonic zone. Figure 11 shows the distribution of the exponential function of entropy. An almost constant value of entropy prevails over most of the surface until the expected position of the recompression shock is approached. Oscillations upstream of the high entropy region are characteristic of the truncated Fourier series representation

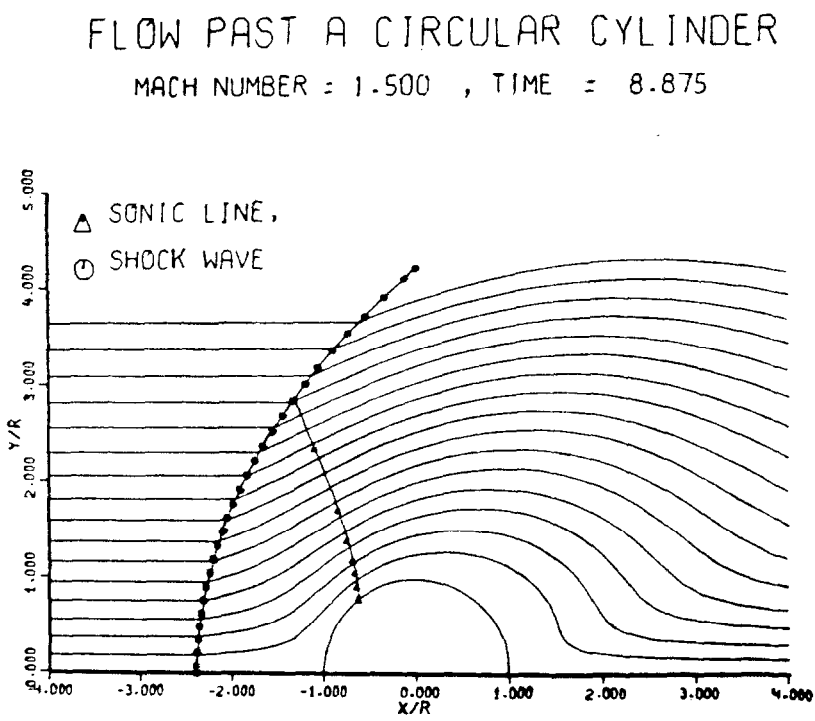

FIG. 9. Instantaneous streamlines, $M = 1.50$, $tU/R = 8.9$.

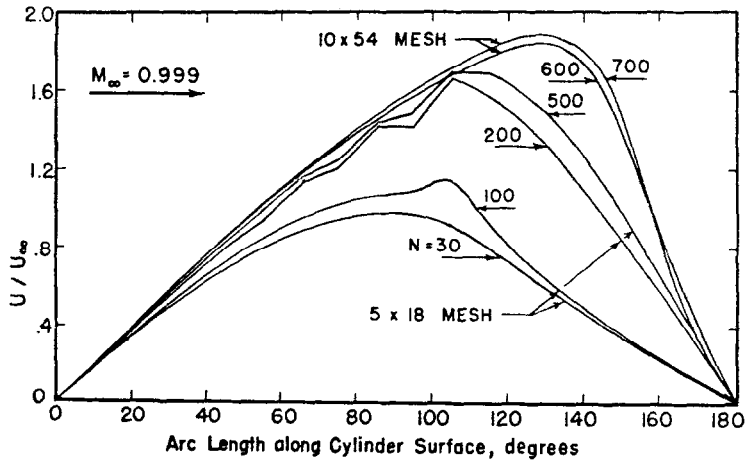

FIG. 10. Velocity distribution as a function of the number of integration steps, N; $M = 0.999$.

of discontinuous functions. A higher numerical dissipation used in the neighborhood of the rear stagnation point smoothed out the oscillations in the high entropy region, but the characteristic overshot at the discontinuity is clearly visible. The fact that the entropy at the front stagnation point is not equal to the free stream value may be explained by the presence of the discontinuity (moving shock wave) in front of the cylinder. At $M = 0.999$ the discontinuity moves in the upstream

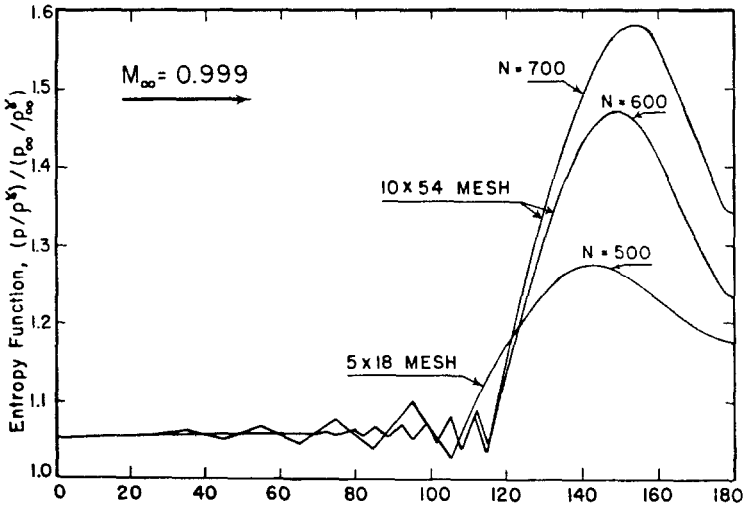

FIG. 11. Entropy distribution on the surface of a circular cylinder as a function of the number of integration steps, N; $M = 0.999$.

direction with a small velocity which diminishes with time at a very slow rate. The shock strength also decreases slowly with time. Consequently, some improvement in accuracy could be realized by carrying out the integration to larger values of time. The condition of the constancy of entropy was not imposed on the system of equations of motion and, therefore, the calculated entropy provides a convenient indication of the accuracy of the solutions. Further, the behavior of entropy is a good indication of the presence or absence of imbedded shocks in the flow field.

DISCUSSION AND CONCLUSIONS

We first observe that it is quite feasible to obtain reasonably accurate solutions to impulsively started flows on an infinite domain using a rather coarse mesh (a maximum of 10×54 mesh points was used). The settling of the flow to a

steady-state condition is quite rapid in the neighborhood of the body. As a consequence of a properly-posed initial-boundary value problem for the hyperbolic system of equations of gasdynamics, the family of solutions for a given body is a continuous function of the free-stream Mach number.

The accuracy of the solution may be increased by employing a much finer mesh. However, the gain in accuracy will not be commensurable with the computing effort expended. The truncation errors of the first-order scheme employed here were reduced to a minimum by using the weight factor σ equal to 0.01 (except in the neighborhood of the shock). Further reduction of the truncation errors results in a trade-off between the accuracy and stability without any improvement in the reliability of the solution. Second-order schemes often need artificially added stabilizing terms which give rise to errors of comparable magnitude. The truncation errors manifest themselves in the phenomenon of the "numerical dissipation" and as such will have an insignificant influence except in regions where second derivatives of the dependent variables are large. In particular, "numerical dissipation" spreads out any gasdynamic discontinuity over a length of about 10 mesh points (3–5 mesh points for second-order schemes). The presence of imbedded shocks in the transonic flow destroys, therefore, the accuracy of the solution. In the case of very thin bodies, such as airfoils, the shock will be weak and it may suffice to use a finer mesh locally in the vicinity of the expected shock position. The best remedy for the present problem of a flow past a circular cylinder would be to introduce a coordinate system such that the shock wave would coincide with a coordinate line. The Rankine–Hugoniot conditions would then govern the motion of the discontinuity in the same manner as the motion of the external boundary was governed in the numerical examples reported here. It is believed that only by treating secondary shocks in the flow field as gasdynamic discontinuities would it be possible to answer with certainty the question whether shock-free transonic flows are possible or not, and whether or not a shock wave assumes a stable position in the absence of a boundary layer on a contour with a continuous curvature.

There remains to comment on the role of a numerical treatment of the boundary conditions. A convergent finite-difference scheme conserves mass, momentum and energy at internal points with predictable and controllable accuracy. The treatment of boundary points is much more critical. Errors at solid boundaries may be interpreted as fluxes of mass, momentum and energy which will have an almost constant and generally small effect at large distances from the boundary. However, an external boundary comprised of a shock will grow with time and any errors in determining accurately the large fluxes there will lead to a rapid, almost exponential growth of the integrals of mass, momentum, and energy balance. This phenomenon, being of a global rather than local nature, was often attributed to a "nonlinear instability." An extensive study of the numerical treatment of

shock motion undertaken by the author led to the conclusion that it is of utmost importance to describe accurately the mechanism by which the flow behind a shock wave determines the shock velocity and, by the Rankine–Hugoniot jump conditions, the flow variables on the downstream side of the shock. Thus, it is mandatory to construct a finite-difference analog of the compatibility relation of the method of characteristics which, together with the jump conditions, determines the shock motion uniquely. The overall accuracy of such an analog need not be higher than that of the finite-difference scheme used for internal points.

Applications of compatibility relations of the theory of characteristics and the Rankine–Hugoniot jump conditions to a multidimensional shock motion are being studied further in an effort to arrive at an exact form of the boundary conditions suitable for a convenient discretization. Results of the research will be reported at a later date.

REFERENCES

1. O. M. BELOTSERKOVSKY, Ed., "Supersonic Gas Flows Around Blunt Bodies," NASA TT F-453 (1967).
2. P. I. CHUSHKIN, Calculation of some sonic flows of a gas, *Prikl. Mat. Meh.* **21** (1957), 353–360.
3. R. E. SINGLETON, "Lax-Wendroff Difference Scheme Applied to the Transonic Airfoil Problem," AGARD Specialists' Meeting on Transonic Aerodynamics, AGARD Conference Proceedings No. 35 (Reprint), September 18–20, 1968.
4. G. MAGNUS, W. GALLAHER, AND H. YOSHIHARA, "Inviscid Supercritical Airfoil Theory," AGARD Specialists' Meeting on Transonic Aerodynamics, AGARD Conference Proceedings No. 35 (Reprint), September 18–20, 1968.
5. C. P. KENTZER, "Computations of Time Dependent Flows on an Infinite Domain," Accepted for Presentation at the AIAA 8th Aerospace Sciences Meeting, January 19–21, 1970, New York.
6. G. MORETTI, "The Importance of Boundary Conditions in the Numerical Treatment of Hyperbolic Equations," PIBAL Report No. 68–34 (1968).